molecular pharmaceutics

Article

pubs.acs.org/molecularpharmaceutics

One Stone Kills Three Birds: Novel Boron-Containing Vesicles for Potential BNCT, Controlled Drug Release, and Diagnostic Imaging

Gaojian Chen,[†,‡] Jingying Yang,[†] Gang Lu,[§] Pi Chu Liu,[§] Qianjin Chen,[†] Zuowei Xie,[†] and Chi Wu*[,†,∥]

[†]Department of Chemistry, The Chinese University of Hong Kong, Shatin, New Territories, Hong Kong

[‡]Center for Soft Condensed Matter Physics and Interdisciplinary Research, Soochow University, Suzhou 215006, P. R. China

[§]Department of Surgery, The Chinese University of Hong Kong, Shatin, New Territories, Hong Kong

[∥]The Hefei National laboratory of Physical Science at Microscale, Department of Chemical Physics, The University of Science and Technology of China, Hefei, Anhui 230026, P. R. China

Supporting Information

ABSTRACT: A new conjugate polymer was prepared by an efficient thiol−ene coupling of one carborane with a linear PEG chain (M_n = 2,000 g/mol), and each carborane was further labeled with a fluorescence rhodamine dye. Such a novel polymer can associate in water to form narrowly distributed spherical vesicles, which were characterized using a range of methods, including laser light scattering, confocal laser scanning microscopy, and TEM. The vesicular structure is potentially multifunctional in biomedical applications, namely, serving as a boron neutron capture therapy (BNCT) agent, a hydrophilic drug carrier, and a diagnostic imaging fluorescent probe. As expected, either cleaving the thiol−ene linked PEO chain by esterase or destroying carborane by neutron irradiation results in a dismantlement of such a vesicle structure to release its encapsulated drugs. Its potential biomedical applications have been evaluated in vitro and in vivo. Our preliminary results reveal that these small vesicles can be quickly taken up by cells and have an enhanced stability in the bloodstream so that their targeting to specific cancer cells becomes feasible.

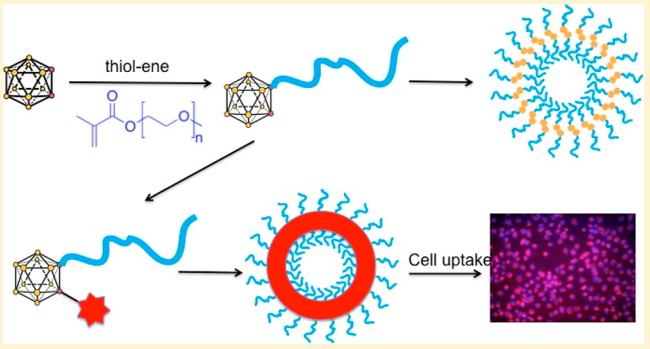

KEYWORDS: *carborane, polymeric vesicles, BNCT, controlled drug release, laser light scattering, diagnostic imaging*

1. INTRODUCTION

Carboranes, an abbreviation of a kind of dicarba-*closo*-dodecaboranes, have been extensively studied in the past 50 years due to their unique physical and chemical properties.[1−3] More specifically, carboranes have a high content of ^{10}B atoms with the highest neutron capture cross section among all light elements. Such a unique property makes them a perfect potential candidate for boron neutron capture therapy (BNCT), a much researched experimental approach for tumor treatment because, when irradiated with low-energy thermal neutrons, each ^{10}B can undergo a nuclear reaction to produce α-particles and recoiling ^{7}Li nuclei.[4,5] These high-energy particles have a short destructive length (5−9 μm), which makes BNCT more clinically appealing because only those cells near boron will be killed. Theoretically BNCT provides a selective destruction of cancer cells while sparing normal ones if we are able to target and concentrate boron containing chemicals inside tumors. In comparison with most small anticancer drugs, carboranes are not chemotherapy agents, with some disadvantages, such as low water solubility, rapid blood clearance, and low tumor selectivity. The solubility problem can be solved by connecting each carborane with some hydrophilic groups, such as carbohydrates, chargeable groups and water-soluble chains.[4,6] The tumor targeting problem is not unique for carboranes and BNCT but generally for many potential cancer therapies.

Clinical interests of BNCT were started with a focus on high-grade gliomas and either cerebral metastases or cutaneous primaries of melanoma.[6] In order to pass the blood−brain barrier (BBB) and reach tumors inside the brain, small molecular BNCT agents were more preferred for a long time. Strategically, such an approach has made a mistake by picking the most difficult problem in treating cancers as its first objective. The unsuccessful story of BNCT has slowly scared away potential funding and hindered further research activities. More recently, BNCT has been used to treat cancers in other parts instead of the brain, making the design of delivery vectors easier.

Special Issue: Recent Molecular Pharmaceutical Development in China

Received: October 31, 2013
Revised: January 18, 2014
Accepted: February 12, 2014
Published: February 12, 2014

On the other hand, it has been extensively displayed that dispersing hydrophobic chemicals, including various drugs, with a proper "surfactant" (small amphiphilic molecules or polymer chains) can enhance their water solubility and stability. In addition, passive or active targeting can further enhance their intracellular uptake in cancer cells and reduce their toxicity.[7−9] As for carboranes, their conjugation with chains has been prepared for different applications.[10−14] As expected, attaching a proper hydrophilic chain on each carborane can lead an amphiphilic hybrid so that these hydrides can self-assemble in water to form some micelle-like structures. In conventional drug-loaded micelles made of amphiphilic diblock copolymers, hydrophobic drugs are physically encapsulated into their hydrophobic core, which often leads to a drug release within a few hours and results in severe potential systemic toxicities.[9] Moreover, it is not easy to quantitatively control the loading of drugs inside micelles. On the other hand, linking drugs to a vector via chemical bonds is more stable and more controllable, but it involves more costly chemical synthesis, separation, and purification.

In BNCT, one has to estimate the boron content inside tumors in real time because the radiation dose is determined by how ^{10}B is microscopically distributed, requiring real time imaging of tumors. Ideally, we would desire a vector that naturally contains as many boron atoms as possible, effectively loads an anticancer drug that can be released by neutron irradiation, and optically or magnetically or radioactively "shines" to indicate its exact location inside the body. Of course, we also prefer to have cheap and easy chemistry in its synthesis. It should be noted that, for biomedical applications, modified amphiphilic carboranes are often associated or aggregated in aqueous solutions to form some nano- or microstructures. Such an association/aggregation process is complicated and often not well governed by thermodynamics, but less attention has been paid to this complicated behavior in spite of the fact that carborane-containing conjugates have been extensively studied in pharmaceutical research.

Bearing these problems in mind, we decided to choose short PEG chains as a hydrophilic stabilizer to develop a novel kind of BNCT vector because PEG chains are biocompatible and approved by the FDA. In this study, a bifunctional thiol terminal carborane was first prepared to generate two −SH groups that are respectively linked with one PEG chain and one fluorescent imaging probe via a thiol−ene addition or click reaction.[15,16] For each reaction, we have two choices: the anti-Markovnikov radical addition[17,18] or the base/nucleophile catalyzed Michael addition.[19−21] We prefer to use the latter approach to click carborane and PEG together because it involves mild reaction conditions, forms minimal byproducts, is tolerant of different functional groups, and yields a high conversion under optimal reaction conditions. To our surprise, such an obtained carborane−PEG conjugate can form small well-defined and narrowly distributed vesicles with a size of ∼80 nm and a ∼10 nm thin fluorescence shell. We also in vitro and in vivo preliminarily evaluated their potential biomedical applications.

2. EXPERIMENTAL SECTION

2.1. Materials and Instruments. 1,2-Bis(mercapto)-*o*-carborane (**1**) was synthesized as reported.[22] Acryloxyethyl thiocarbamoyl rhodamine B was from Polysciences Inc., Warrington, PA, USA. All other chemicals were from Sigma-Aldrich and used as received. NMR spectra were recorded on a Bruker 400 MHz spectrometer, and deuterated chloroform was used as solvent. GPC characterization was carried out using an Agilent PL-50 size exclusion chromatograph (SEC) equipped with a refractive index detector, using PL Mixed gel C (5 mm beads size) columns with their molar mass ranging from 200 to 2×10^6 g/mol. THF was used as the eluent with a flow rate of 1.0 mL/min at 40 °C. Transmission electron microscopy (TEM) imaging was obtained using an FEI CM120 microscope operated at 120 kV. Each sample was prepared by placing a drop of the solution onto a carbon-coated copper grid and dried in two methods. Method 1: Wait for 1 min to let the nanocapsules bind to the carbon membrane; blot with filter paper; dry naturally in air at room temperature. Method 2: After the sample solution was dropped to the copper grids in a small vial that was chilled with liquid nitrogen, the solvent was removed by freeze-drying under high vacuum. TEM results from these two methods were compared. Confocal laser scanning microscopy was performed using a Nikon C1si CLSM equipped with a fluorescent imaging detector (Nikon, Japan). Rhodamine-labeled carborane−PEG vesicles in water were visualized at 543 nm, and their fluorescence was acquired by a 605/75 detectors and analyzed using Nikon EZ-C1 software. The UV−vis spectra were taken using a Shimadzu (Kyoto, Japan) UV-3600. The fluorescence spectrum was recorded on a Hitachi F-7000 spectrofluorometer, and the emission spectrum of a rhodamine B solution (2.5 μg/mL) at different pH values was measured at 543 nm, identical as that used in the confocal microscope measurements. Atomic force microscopy (AFM) was performed using Asylum Research MFP-3D-Bio. The samples were prepared by dropping the vesicle solution onto a silicon wafer and freeze-drying and were imaged in air in the tapping mode using a silicon cantilever with a typical tip radius of around 10 nm.

2.2. Synthesis of Carborane−PEO Conjugate. Poly(ethylene glycol) methyl ether methacrylate with a molecular weight of 2000 ($PEGMEMA_{2000}$) was purchased from Aldrich (50 wt % in H_2O). Water was removed by freeze-drying, and the polymer was used directly without further purification. As shown in Scheme 1, PEG modified carborane was obtained via the reaction between the thiol-terminal carborane **1** and

Scheme 1. Synthesis of Carborane−PEG Conjugate and Rhodamine Labeling[a]

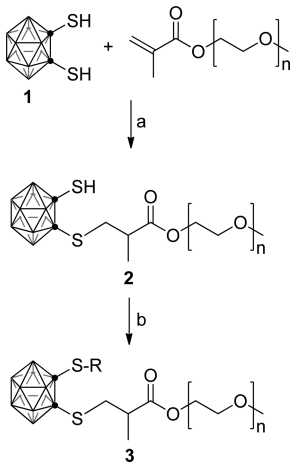

[a](a) Hexylamine, THF; (b) methacryloxyethyl thiocarbamoyl rhodamine B, hexylamine, THF.

$PEGMEMA_{2000}$. The procedure is outlined as follows. $PEGMEMA_{2000}$ (80 mg, 0.04 mmol) was added into 2 mL of THF and purged with nitrogen for 10 min, to which were added thiol-functional carborane **1** (16 mg, 0.08 mmol) and *n*-hexylamine (5 μL, 0.04 mmol). The reaction mixture was stirred at room temperature for 48 h, then precipitated into diethyl ether three times, and dried under vacuum to afford polymer **2**. ^{1}H NMR (400 MHz, $CDCl_3$, 25 °C): δ (ppm) 4.5−4.3 (2H, $COOCH_2CH_2O$), 3.9−3.5 (4*n*H, OCH_2CH_2O), 3.5 (1H, CH_3CH), 3.3−3.4 (3H, OCH_3), 3.3−3.0 (2H, SCH_2), 1.7−1.5 (1H, −SH), 1.4−1.2 (3H, $CHCH_3$).

In the reaction between **1** and $PEGMEMA_{2000}$, catalysts play an important role for efficient coupling via the Michael addition thiol−ene reaction.[23] Normally, a weak base catalyst such as triethylamine is sufficient to catalyze a traditional Michael addition reaction. However, reports have shown that a simple primary amine such as hexylamine provides a much faster reaction rate.[15] Figure S1 in the Supporting Information shows the disappearance of the peaks at 1.9, 5.4, and 6.1 ppm, which corresponds to the methyl and acetylene groups of $PEGMEMA_{2000}$, after 24 h at 25 °C when hexylamine was used. On the contrary, less than 1% conversion was achieved when triethylamine was used as a catalyst under the same conditions. Hexylamine was then chosen as the catalyst of the thiol−ene reaction in the current study, and the complete conversion was confirmed by ^{1}H NMR spectra.

The conjugate **2** was further labeled with rhodamine. Acryloxyethyl thiocarbamoyl rhodamine B (10 mg, 15 μmol) and **2** (22 mg, 10 μmol) were dissolved in 1 mL of THF and purged with nitrogen for 10 min before addition of *n*-hexylamine (1.2 μL, 10 μmol). The reaction was stirred at room temperature for 48 h. The resultant solution was then diluted with water, transferred into a MWCO 1000 dialysis bag, and dialyzed against 2 L of water three times; the final solution was lyophilized to afford **3**. 72% functionalization of rhodamine was obtained on the basis of the integrations between ^{1}H NMR peaks of aromatic protons of rhodamine B and the CH_2 peaks near the ester bond from both rhodamine B and $PEGMEMA_{2000}$.

2.3. Laser Light Scattering (LLS). A modified commercial LLS spectrometer (ALV/DLS/SLS-5022F) equipped with a multi-τ digital time correlator (ALV5000) and a cylindrical 22 mW UNIPHASE He−Ne laser (λ_0 = 632 nm) was used. The incident beam was vertically polarized with respect to the scattering plane. The details of the LLS instrumentation and theory can be found elsewhere.[24,25] In static LLS, the excess absolute time-averaged scattered light intensity, known as the excess Rayleigh ratio $R_{vv}(\theta)$, at a given polymer concentration (C) and a given scattering angle (θ) is related to the weight-average molar mass (M_w), the square average radius of gyration ($\langle R_g^2 \rangle$), and the second virial coefficient (A_2) as

$$\left[\frac{KC}{R_{vv}(\theta)}\right] \approx \frac{1}{M_w}\left(1 + \frac{1}{3}\left\langle R_g^2 \right\rangle q^2\right) + 2A_2C \quad (1)$$

where $K = 4\pi^2 n^2 (dn/dC)^2/(N_A \lambda_0^4)$ with N_A and dn/dC, the Avogadro number and the specific refractive index increment, respectively.

In dynamic LLS, each measured $G^{(2)}(q,t)$ is related to the normalized electric field−field time correlation function $g^{(1)}(q,t)$ by $G^{(2)}(q,t) = A[1 + b|g(1)(q,t)|^2]$, where A is a baseline; $0 \le b \le 1$, a spatial coherent constant depending on the instrumental detection optics. The value of b actually reflects the signal-to-noise ratio of a dynamic light-scattering experiment. It has been shown that $|g^{(1)}(q,t)|$ is proportional to $S(q,t)$ and related to the characteristic line-width distribution $G(\Gamma)$ by[25]

$$g^{(1)}(q, t) = \int_0^\infty G(\Gamma)\, e^{-\Gamma t} d\Gamma \quad (2)$$

The Laplace inversion of each measured $g^{(1)}(q,t)$ leads to one $G(\Gamma)$ on the basis of eq 2. In this study, the CONTIN algorithm in the digital time correlator was used. For a pure diffusive relaxation, such as for narrowly distributed polymer chains or spherical colloidal particles in a dilute solution or dispersion at $x \ll 1$, $G(\Gamma)$ can be converted into a translational diffusion coefficient distribution $G(D)$ by $D = \Gamma/q^2$ or further to a hydrodynamic radius distribution $f(R_h)$ by using the Stokes−Einstein equation.

2.4. Preparation of Spherical Vesicles. 10 mg of **2** or **3** was added into a round-bottom flask containing THF, the solvent was removed by rota-evaporation, and 10 mL of deionized water was added to afford the 1 mg/mL solution. The mixture was stabilized for 24 h and diluted into different concentration for LLS analysis. Procedure for fluorescence quenching: 2 mg of **2** was dissolved into 6 mL of 2.5 μg/mL rhodamine B water solution. The mixture was stirred in the dark for one hour and stabilized overnight. 20 μL of the above prepared solution was dropped onto a precleaned glass slide, confocal images were taken with proper settings, and then 2 μL of concentrated HCl was dropped into the solution and let stabilize for 10 min; the confocal images were taken again with the same settings as before.

2.5. Drug Loading Studies. Rhodamine B was used as a model hydrophilic drug for loading experiment. Typical procedure for the preparation of nanocapsules of **2** loaded with rhodamine B: 5.2 mg of **2** was dissolved into 9 mL of 0.2 mg/mL rhodamine B water solution. The mixture was stirred in the dark for one hour and then dialyzed against 2 L of water using a MWCO 3500 dialysis bag, and water was changed five times.

For drug release studies, the in vitro release of DOX·HCl from vesicles was studied using a dialysis bag (MWCO 3500) at 37 °C in PBS (10 mM, pH 7.4). 2 mL of pH 7.4 PBS solution (DOX at 100 μg/mL, and polymer at 306 μg/mL) was dialyzed against 200 mL of the same medium. At desired time intervals, 3 mL of the release medium was taken out and replenished with an equal volume of fresh medium. The amount of DOX released was determined by using a fluorescence spectrometer (Hitachi F-7000) at 500 nm (excitation) and 580 nm (emission). The amount released was then calculated. Esterase (30 units) was added into the dialysis bag when the DOX release at the same condition was studied.

2.6. MTT Cell Viability Assay. The cytotoxicity assessment was carried out on HepG2 cells by using the MTT assay. HepG2 cells were seeded in a 96-well plate at an initial density of 6000 cells/well in 100 μL of the DMEM complete medium. After 24 h, the cells were treated with polymers at different concentrations. The treated cells were incubated in a humidified environment with 5% CO_2 at 37 °C for 48 h. The MTT reagent (in 20 μL of PBS, 5 mg/mL) was added to each well. The cells were further incubated for 4 h at 37 °C. The medium in each well was then removed and replaced by 100 μL of DMSO. The plate was gently agitated for 15 min before the absorbance (A) at 490 nm was recorded by a microplate reader (Bio-Rad). The cell viability (x) was

calculated by $x = A_{490,\text{treated}}/A_{490,\text{control}} \times 100\%$, where $A_{490,\text{treated}}$ and $A_{490,\text{control}}$ are the absorbance values of the cells cultured with and without PDMAEMA, respectively. Each experimental condition was done in quadruplicate. The data are shown as the mean value plus a standard deviation (±SD).

2.7. Cellular Uptake Observed with Fluorescence Microscopy. U87 cells were plated onto a 12-well plate at 50,000 cells per well in 2 mL of DMEM medium supplemented with 10% FBS. They were incubated for 24 h at 37 °C and 5% CO_2 before treatment. The PEG−carborane nanocapsule solution was prepared in PBS at pH 7.4. To each well was added 20 μL of the nanocapsule solution. The images were taken 4 h later using a fluorescent microscope (Nikon Inverted Research Microscope Eclipse TE2000). 4′,6-Diamidino-2-phenylindole (DAPI, Invitrogen) was added to the wells at a concentration of 5 μM before images were taken.

2.8. In Vivo Studies. All the procedures were approved by the Animal Experiment Ethics Committee of the Chinese University of Hong Kong. Adult male mice were adapted to the environment for one week and allowed access to chow and water ad libitum. Carborane polymer saline solution (8 mg/kg) was injected into each mouse intravenously. The blood samples of the mice were collected at different time points (0.1, 0.5, 1, 3, 6, 12, 24, 48 h) after injection. All samples were anticoagulated by EDTA and stored at 4 °C until further experiment. The ICP-OES method was used to monitor the boron content: a procedure similar to one previously reported was used.[26] Whole blood samples (100 μL) were added into polypropylene tubes and deproteinized by adding 2 mL of 0.4 mol/L trifluoroacetic acid solution under continuous mixing. After short centrifugation (2900*g*; 3 min), the clear supernatant was aspirated into a Perkin-Elmer Optima 4300 DV ICP-OES instrument after calibration using boron standard solutions. Aqueous calibrators for boron were diluted to 0.1−50 mg/L and treated as samples. The results of the boron content were presented as percentage of total injected polymer, by assuming that the total volume of blood was 7.6% of the body weight.[27] Each experimental condition was done in quadruplicate. The data are shown as the mean value plus a standard deviation (±SD).

At the end of the blood collection, the mice were sacrificed and infused with normal saline to replace the blood of mice. Then, all organs of mice (brain, heart, lung, liver, spleen, and kidney) were collected. The fluorescent images of organs were detected by in vivo imaging system IVIS 200 (Caliper, Hopkinton, MA). The parameters of IVIS 200 were as listed below: excitation filter GFP (445−490 nm), emission filter GFP (515−575 nm), fluorescence level high, field-of-view 22 cm, *f*-number 8, exposure time 3 s. The mouse injected with normal saline intravenously was regarded as control.

3. RESULTS AND DISCUSSION

Knowing the morphology of amphiphilic polymer chains in selective solvents, especially in aqueous solutions, is not only important but also the first step for any of their biorelated potential applications. It is well-known that they tend to self-assemble in a selective solvent to form spherical and cylindrical micelles, and sometimes vesicles, depending on their detailed molecular characteristics, including the amphiphilic contrast, comonomer distribution, and the lengths of different segments. Here, the carborane−PEG conjugate **2** is like a large surfactant but in an opposite way; namely, instead of a hydrophilic head, it has a hydrophilic tail longer than most of small molecule surfactant and a hydrophobic carborane head. Therefore, we started with a laser light-scattering study of its morphology in water. The average characteristic line width ($\langle\Gamma\rangle$) of the carborane−PEG conjugate **2** in water, measured by dynamic LLS, is a linear function of the square of the scattering vector (q^2) with its extrapolation ($q \to 0$) passing through the origin, indicating that the relaxation is diffusive. (Figure S5 in the Supporting Information). The slope leads to an average translational diffusion coefficient ($\langle D\rangle = 2.76 \times 10^{-12}$ m^2/s) that can be converted to an average hydrodynamic radius by using the Stokes−Einstein equation. Our results also showed that the measured average line width is nearly independent of the polymer concentration (C) in the range 10^{-4}−10^{-3} g/mL.

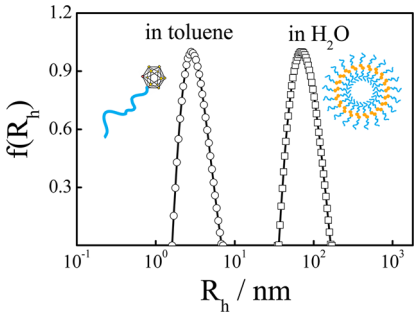

Figure 1. Typical normalized hydrodynamic radius (R_h) distributions of carborane−PEG **2** in toluene (1 mg/mL) and in water (0.1 mg/mL), where $\theta = 90°$ and $T = 25$ °C.

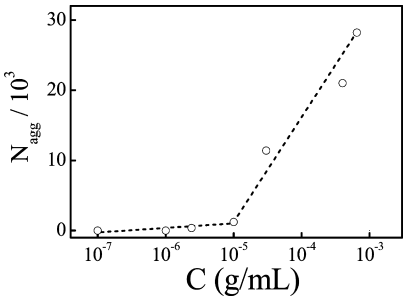

Figure 2. Polymer concentration (C) dependence of average aggregation number (N_{agg}) of carborane−PEG conjugate **2** in water.

Figure 1 shows two typical normalized hydrodynamic radius (R_h) distributions of the carborane−PEG conjugate **2**, respectively, in toluene (1×10^{-3} g/mL) and in water (1×10^{-4} g/mL) from their corresponding line-width distributions. As expected, the conjugate **2** should exist as individual random-coiled chains in a common good solvent (toluene), which is confirmed by the narrowly distributed peak located at $\langle R_h\rangle$ = 2.9 nm. While in water (a solvent only selectively good for PEG), we observed something much larger, represented by the peak located at $\langle R_h\rangle \approx 73$ nm with a relative width of $\mu_2/\langle\Gamma\rangle^2 \approx 0.1$. Presumably, the peak is related to the association of the conjugate chains in water.

The next question is to which morphology individual conjugate **2** chains are associated together in water and how many of them are inside each self-assembled structure. To answer these questions, we performed static LLS; namely, we measured the absolute scattered light intensity. A typical plot of $KC/R_{vv}(q)$ vs q^2 for a given dilute solution can be found in Figure S6 in the Supporting Information. As described in eq 1, its intercept and slope led to a weight-averaged molar mass ($M_w \sim 5.1 \times 10^7$ g/mol) and an average radius of gyration ($\langle R_g\rangle \sim$ 79 nm) of the self-assembled structure, respectively, after

Table 1. Light Scattering Characterization of Carborane−PEG Conjugate 2 in H_2O at 25 °C

C, g/mL	M_w, g/mol	$\langle R_g \rangle$, nm	$\langle R_h \rangle$, nm	$\langle R_g \rangle / \langle R_h \rangle$	$\langle R_g \rangle_{cal}$, nm	$\langle R_g \rangle_{cal} / \langle R_h \rangle$	N_{agg}	σ, nm^2/PEG
6.5×10^{-4}	5.1×10^7	79	87	0.92	81	0.93	2.8×10^4	5.8
4.0×10^{-4}	4.6×10^7	91	93	0.97	87	0.94	2.1×10^4	9.2
2.0×10^{-5}	1.4×10^7	91	89	1.02	83	0.94	1.3×10^4	13.8

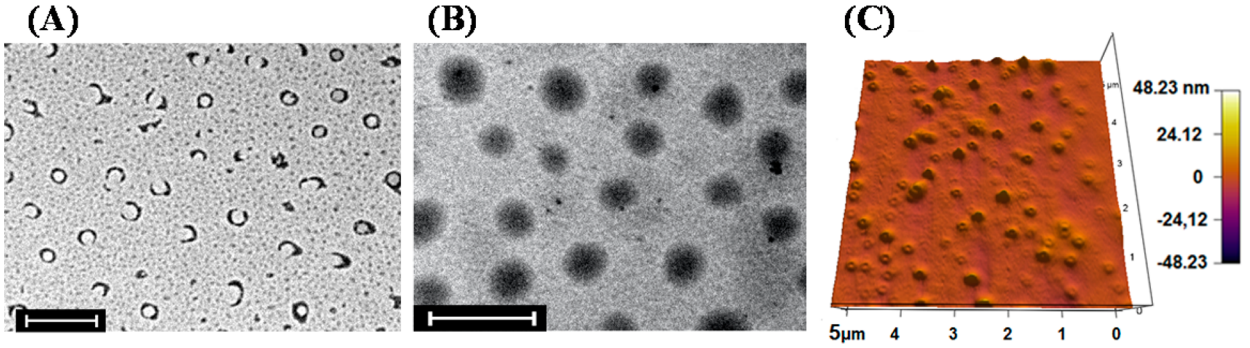

Figure 3. (A) TEM image of vesicular structures of carborane−PEG conjugate **2** in aqueous solution prepared by freeze-drying method. (B) TEM image of carborane−PEG conjugate **2** in aqueous solution prepared by drying at atmosphere. (C) AFM 3D topographic image of carborane−PEG conjugate **3** in aqueous solution. Scale bars are (A) 500 nm and (B) 400 nm.

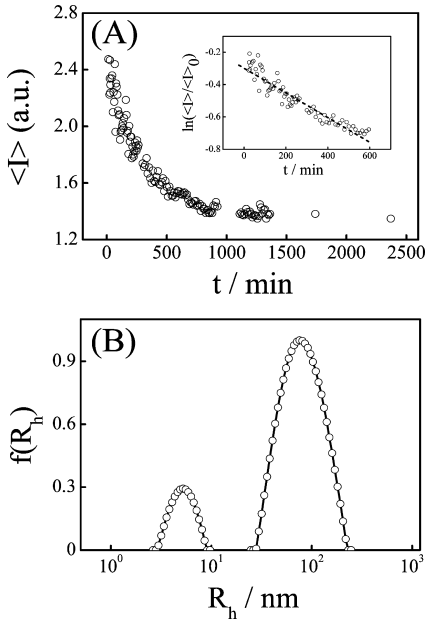

Figure 4. (A) Enzyme cleavage kinetics of vesicles made of carborane−PEG conjugate **2** in PBS buffer (pH = 7.4), where the inset shows a semilogarithmical plot. (B) Hydrodynamic radius distribution of carborane−PEG conjugate **2** in PBS buffer (pH = 7.4) after 24 h enzyme cleavage.

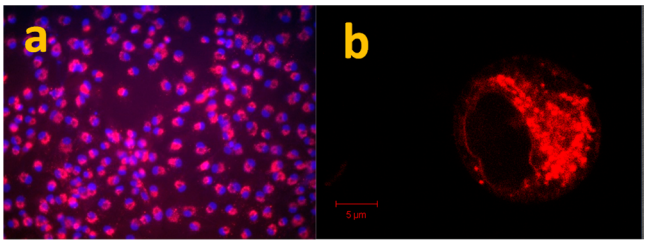

Figure 5. (a) Fluorescence images of U87 cells after their uptake of vesicles made of rhodamine B-carborane−PEG conjugate **3**, where nucleuses are stained with DAPI. (b) Confocal microscopy images of Hela cells after uptake of vesicles made of polymer **3**.

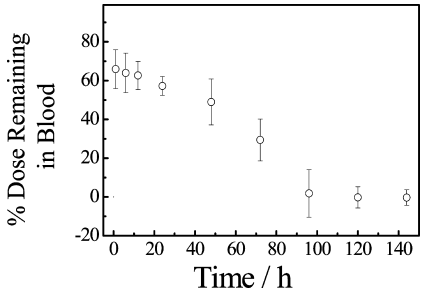

Figure 6. Time dependence of total boron in whole blood of mice after it was injected with a saline solution of vesicles made of rhodamine B-carborane−PEG conjugate **3** at 8 mg per kg of mouse weight. The amount of boron in mice prior to injection of the formulation has been used as control to calculate the dose remaining in blood.

ignoring a small contribution of the concentration term. Note that the dn/dC used is 0.212 mL/g, measured by using a novel differential refractometer.[28] By knowing M_o (2.21×10^3 g/mol) of individual conjugate chains, we can estimate the average aggregation number (N_{agg}, 2.8×10^4) from the ratio of M_w/M_o.

Further dilution leads to a decrease in the concentration-normalized scattering intensity, i.e., a smaller aggregation number (N_{agg}), as shown in Figure 2. It clearly shows that N_{agg} increases dramatically when C is higher than the critical aggregation concentration (CAC, 1×10^{-5} g/mL). If a spherical polymeric micelle was formed, it would be difficult to imagine how ~10^4 chains could be packed together when C > CAC because its carborane core simply had no sufficient surface area to accommodate ~10^4 PEG chains on its periphery (in its shell). It is known that the ratio of $\langle R_g \rangle / \langle R_h \rangle$ is closely related to the density distribution of a scattering object in space. For example, for a random coil chain, a thin-shell hollow sphere, and a hard sphere, $\langle R_g \rangle / \langle R_h \rangle$ ~ 1.5, 1.0, and 0.776, respectively.[29−31]

Table 1 summarizes the LLS results for the carborane−PEG conjugate **2** in water. It shows that when $C > 1 \times 10^{-5}$ g/mL, $\langle R_g \rangle / \langle R_h \rangle$ ~ 1, indicating the formation of a liposome-like

dx.doi.org/10.1021/mp400641u | Mol. Pharmaceutics 2014, 11, 3291−3299

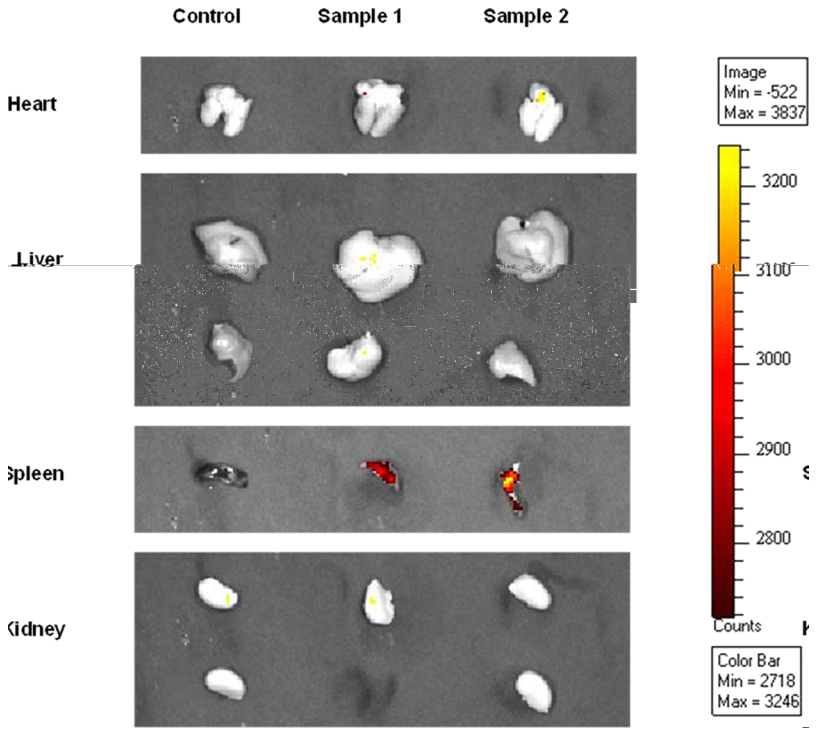

Figure 7. Biodistribution of rhodamine B-carborane−PEG conjugate 48 h after intravenous injection of a saline solution of polymer **3**.

structure. Note that such vesicular structures have been found before in the study of PEG chains with a bulky hydrophobic end, such as camptothecin and fullerenein, in water.[20,32] To form such a vesicular structure, the hydrophobic carborane heads associate together to form a double layer, as schematically shown in Figure 1. We know that each conjugate chain has an average size of ∼5.8 nm in good solvent. Therefore, each vesicle should have a thin shell of 11−12 nm. Taking each vesicle as a hollow sphere with $\langle R_h \rangle$ as its radius and a 11−12 nm thin shell, we can calculate its radius of gyration ($\langle R_g \rangle_{cal}$) and radius ratio ($\langle R_g \rangle_{cal}/\langle R_h \rangle$) from its definition, as shown in Table 1, close to those measured from static LLS.

Further, we can also estimate the average surface area (σ) occupied by each PEG chain from the total surface area ($4\pi R^2$) and half of the aggregation number (N_{agg}), also summarized in Table 1. Note that *o*-carborane has a diameter of ∼0.8 nm so that its cross section is ∼2 nm^2. On the other hand, each coiled PEG chain has a radius of gyration of $\langle R_g \rangle \sim 4.4$ nm so that its cross section is ∼60 nm^2, much larger than those values estimated from our LLS results. Such a difference in σ indicates that PEG chains are much stretched on the periphery. Also note that both N_{agg} and $\langle R_h \rangle$ increase and σ decreases as C increases from 2.0×10^{-4} g/mL to 4.0×10^{-4} g/mL, which is expected because more conjugate chains are packed into each vesicle and each PEG chain is more stretched. The stretch of PEG outside increases both $\langle R_h \rangle$ and $\langle R_g \rangle$, but the stretch of PEG inside should have no effect on $\langle R_h \rangle$ but decrease $\langle R_g \rangle$. This is why $\langle R_h \rangle$ increases but $\langle R_g \rangle$ remains. However, it is more surprising to see that both $\langle R_g \rangle$ and $\langle R_h \rangle$ decrease when C further increases from 4.0×10^{-4} g/mL to 6.5×10^{-4} g/mL, indicating that PEG chains collapse when the surface density is sufficiently high.[33,34]

The vesicular structure formed in water was further confirmed by transmission electron microscope (TEM). Figure 3A shows a typical image of the carborane−PEG conjugate **2** in water at 0.05 g/L, where the TEM sample was freeze-dried to avoid the solvent evaporation induced structure collapse. The analysis of TEM images of these vesicles generates a number-average radius of $\langle R \rangle_{TEM} \sim 58$ nm, smaller than the hydrodynamic radius measured in dynamic LLS. This is understandable because $\langle R_h \rangle$ is intensity-weighted so that larger ones weigh much more and the dry-induced shrinkage of the stretched PEG chains certainly decreases $\langle R \rangle_{TEM}$. It should be stated that different morphologies can be observed if different drying processes were used (Figure 3B). A similar phenomenon was also observed for amphiphilic diblock copolymers and highlighted in a previous report.[35]

Since one carborane has two thiol groups, when one is linked with a PEG chain, the other can be further functionalized. In the current study, it reacted with rhodamine-acrylate using hexylamine as a catalyst via the thiol−ene coupling reaction to form the rhodamine B-carborane−PEG conjugate **3**, as shown in Scheme 1. Conjugate **3** aggregates in water and forms vesicles as shown in Figure 3C, where the hollow spheres collapse into bowl-like shapes. DLS measurements (Malvern Zetasizer Nano-ZS90 with narrow band filters) reveal that the size of the aggregate of polymer **3** (∼171 nm) in water is slightly bigger than that that of polymer **2** (∼160 nm), and the CAC of the aggregate (3×10^{-5} g/mL) is also slightly higher. (Figure S7 in the Supporting Information). In principle, other small optical, magnetic, and irradiation probes can also be coupled with a similar strategy without any foreseeable problems. This attached fluorescence probe enables us to monitor the in vivo distribution of the vesicles made of the rhodamine B-carborane−PEG conjugate **3** before applying the neutron irradiation in potential clinical applications.

Moreover, we used the fluorescence quenching to further verify the vesicular structure. It has been known that rhodamine B, a widely used hydrophilic dye, is pH sensitive. Its fluorescence intensity remains in the range pH > 2 but

dramatically decreases when pH < 2 (Figure S8A in the Supporting Information). Therefore, we dissolved the carborane−PEG conjugate **2** in an aqueous solution (pH = 8.6) of rhodamine B. The formation of vesicles encapsulated a certain amount of rhodamine B inside so that their cores emit fluorescence, as shown in Figure S8B in the Supporting Information. After adjusting pH to 0.1 and assuming that protons are not able to diffuse into these vesicles by passing through the shell made of highly packed conjugate chains, we should only see the quench of fluorescence intensity outside (solution) but not inside each vesicle. Figure S8C in the Supporting Information shows our expected result, further confirming the formation of vesicular structure.

Also taking rhodamine B as a model drug, we used a dialysis method similar to loading drugs into conventional liposomes to test feasibility of encapsulation of hydrophilic drugs with these novel vesicles. In this test, 1.8 mg of rhodamine B and 5.2 mg of PEG−carborane were dissolved in 6 mL of water. We found that 10.7% of rhodamine B was loaded. In theory, assuming that the concentration of hydrophilic molecules loaded inside the vesicle is equal to the concentration outside the vesicle, the loading efficiency ($E_{loading}$) is the ratio of internal volumes ($V_{vesicle}$) of all the vesicles to the solution volume ($V_{solution}$), i.e., $E_{loading} = V_{vesicle}/V_{solution}$ and $V_{vesicle} = v_{vesicle}n_{vesicle}$, where $v_{vesicle}$ and $n_{vesicle}$ are the internal volume of each vesicle and the number of the vesicles in the solution, respectively. Knowing the concentration and average molar mass of the conjugate **2** as well as the average aggregation number and size of the vesicles, we can estimate both $v_{vesicle}$ and $n_{vesicle}$. The theoretical maximum loading efficiency is 11%, showing that we nearly reached the theoretical limit at this concentration. Further increase of the carborane−PEG conjugate's concentration can enhance the loading efficiency. As shown in Figure S9 in the Supporting Information, the loading of rhodamine B is directly observed as bright fluorescent cores.

Such carborane−PEG conjugate **2** itself is very stable in water with no noticeable size change over weeks at $C \leq 1$ mg/mL. As expected, with the removal of either the hydrophobic carborane head or the hydrophilic PEG tail, individual vesicles will be dismantled to release their encapsulated "drugs". Since carborane used here is not neutron-active and there is not an accessible neutron irradiation source, we decided to test the controlled release experiment by using esterase to hydrolyze the thioester bond that links one carborane to one PEG chain, namely, the removal of PEG. Note that esterase is abundant in cells. The dismantlement can be effectively monitored by a decrease in the scattering intensity.

Figure 4A shows such a kinetic study of the dismantling process. The scattering intensity $\langle I \rangle$ quickly decreases in the first few hours before slowing down and leveling off at ∼10−20 h. The inset reveals that $\langle I \rangle$ actually exponentially decreases as t increases, indicating that the dismantlement follows first-order kinetics. The rationale is as follows. In the presence of large vesicles, individual PEG chains scatter insignificantly little light so that we can attribute most of the scattered light from large vesicles, i.e., $\langle I \rangle \sim n_{vesicle}M_{vesicle}^2$. Therefore, we have $d\langle I \rangle/dt \propto dn_{vesicle}/dt$ and $dn_{vesicle}/dt = kn_{vesicle}$, i.e., $\ln(n_{vesicle}/n_{vesicle,0}) = -kt$ or $\ln(\langle I \rangle/\langle I \rangle_0) = -kt$, where k is a rate constant, the subscript "0" denotes $t = 0$, and $M_{vesicle}$ is nearly a constant and only slightly varies with time. The estimated k is 7.65×10^{-4} min^{-1}.

Finally, the solution was clarified with a 450 nm membrane filter to remove the insoluble carborane precipitates and characterized by dynamic LLS. Figure 4B shows two peaks in the hydrodynamic radius distribution. The peak located at ∼5 nm reflects individual PEG chains cleaved from the conjugate, while the peak centered at ∼80 nm shows some remaining vesicles. Note that the area under each peak represents the intensity contribution, and the area ratio of the two peaks is ∼14:86. Also note that each vesicle scatters 10^8 times more light than individual PEG chains. In other words, after the enzyme treatment, the number ratio of vesicles/PEG to PEG chains is $\sim 10^8$ and the esterase cleavage is nearly 100% within 24 h. Water-soluble DOX·HCl were further loaded into vesicles of both polymers **2** and **3**. The nanocapsules released DOX·HCl in a controlled manner (Figure S11 in the Supporting Information), suggesting that the water-soluble DOX·HCl has to slowly diffuse out through the hydrophobic membrane made of carborane. With esterase added, polymer **2** nanocapsules release much faster than polymer **3**; likely the interaction of enzyme on the PEG−carborane linkage is slower due to steric hindrance of rhodamine.

Figure 5a shows that these novel vesicles made of rhodamine B-carborane−PEG conjugate chains are quickly taken up by the U87 cells. Most of the cell is fully colored with red rhodamine B except the nucleus, clearly indicating that small vesicles can penetrate the cell membrane but not the nuclear membrane. Confocal fluorescence microscopy was also used to observe the subcellular localization of vesicles made of polymer **3** in Hela cells (Figure 5b and Figure S12 in the Supporting Information); after two hours of incubation, big punctate and small dots were both observed, indicating that rhodamine B-carborane−PEG conjugates were taken up possibly by a combination of endocytosis and diffusion of free chains. Before in vivo animal tests of these vesicles made of carborane−PEG conjugates, we first checked their cytotoxicity by the MTT assay. Figure S10 in the Supporting Information clearly shows that the rhodamine B-carborane−PEG conjugate **3** has nearly no cytotoxicity, in the tested concentration range, very similar to biocompatible PEG, presumably due to the shielding of PEG chains on their periphery.

One of the problems associated with the delivery of boron to targeted tumors is to increase their circulation time, namely, to avoid a possible rapid clearance by the reticuloendothelial system (RES) before they are accumulated on targeted tumors. Figure 6 shows that most of the in vivo administrated carborane−PEG conjugates remain in circulation after one day and 40% of them are still circulating inside even after two days. The level of the remaining conjugates dropped faster afterward and then disappeared after four days. Due to its insolubility in water, we are not able to do a control experiment by using thiol-carborane before its PEGylation. In the literature, 42% of BPA remains in blood after 5 h[26] and only 20% of BSH were left after 24 h even using PEG-liposomes as its carriers.[27] Although they are different from the carborane−PEG conjugates used in the current study, our result clearly shows that the undesired uptake of carboranes by RES has been significantly reduced when they are protected by a PEG shell. Our results are even better than those for PEG-liposomes, presumably because vesicular structures are strongly held together by strong hydrophobic interaction among carboranes and each PEG chain is covalently linked to a carborane.

Further, we checked the biodistribution of the conjugates inside mice by using fluorescent microscopy after intravenous injection of a saline solution of rhodamine B-carborane−PEG conjugate **3** at 8 mg per kg of mouse weight. Figure 7 shows the images taken two days after the administration. It is clear that

some of the rhodamine B-carborane−PEG conjugate **3** was accumulated in spleen, similar to previously reported results for carborane-containing polymers,[36] but not in other organs. Combining with the data of boron content in the bloodstream, the results demonstrate that the conjugate is a good candidate for drug delivery.

4. CONCLUSION

The thiol−ene coupling reaction can be used to make carborane−PEG_{2000} conjugates. Using a range of characterization methods, we have found that these conjugates above their critical aggregation concentration (CAC ∼ 1×10^{-5} g/mL) can self-assemble into very narrowly distributed spherical vesicles with a size smaller than 200 nm. The thiol−ene linkage can be easily cleaved by esterase within 24 h, leading to the dismantlement of the vesicles and the aggregation of carborane molecules, which is beneficial for boron neutron capture therapy (BNCT). The conjugates can be further labeled with one fluorescent rhodamine for imaging and monitoring. Preliminary results show that the PEGlyation makes carboranes nearly nontoxic and their cellular uptake much easier. The in vivo tests by intravenous injection reveal that the formation of vesicles significantly improves their circulation time. Besides fluorescence, our method can also be used to link other labeled probes, such as magnetic and radioactive, and targeting molecules to carboranes. The combination of thiol−ene reaction and a carborane with two thiol groups enables us to use one stone to kill three "birds": BNCT, controlled drug release, and diagnostic imaging.

■ ASSOCIATED CONTENT

Ⓢ Supporting Information

NMR spectra, GPC traces, scattering vector plots, DLS and CAC characterization, emission spectra, confocal images, MTT assay results, and DOX·HCl release kinetics. This material is available free of charge via the Internet at http://pubs.acs.org.

■ AUTHOR INFORMATION

Corresponding Author

*The Hong Kong address should be used for all correspondence. Tel: (+852) 3943 6106. Fax: 2603 5057. E-mail: chiwu@cuhk.edu.hk.

Notes

The authors declare no competing financial interest.

■ ACKNOWLEDGMENTS

The financial support of the Ministry of Science and Technology of China (2012CB933802), the National Natural Science Foundation of China (NSFC) (Project No. 21004042, 51273091 and 51173177), and the Research Grants Council of the Hong Kong Special Administration Region (Project No. CUHK 7/CRF/12G) is gratefully acknowledged. We also wish to thank Professor Yun Zhao and his co-workers for helping us to do some of the in vivo experiments.

■ REFERENCES

(1) Davidson, M. G.; Wade, K.; Marder, T. B.; Hughes, A. K. *Contemporary Boron Chemistry*; Royal Society of Chemistry: Cambridge, 2000.

(2) Fox, M. A. Polyhedral Carboranes. In *Comprehensive Organometallic Chemistry III*; Robert, H. C., Mingos, D. M. P., Eds.; Elsevier: Oxford, 2007; pp 49−112.

(3) Hawthorne, M. F.; Maderna, A. Applications of Radiolabeled Boron Clusters to the Diagnosis and Treatment of Cancer. *Chem. Rev.* **1999**, *99*, 3421−3434.

(4) Valliant, J. The medicinal chemistry of carboranes. *Coord. Chem. Rev.* **2002**, *232*, 173−230.

(5) Armstrong, A. F.; Valliant, J. F. The bioinorganic and medicinal chemistry of carboranes: from new drug discovery to molecular imaging and therapy. *Dalton Trans.* **2007**, 4240−4251.

(6) Barth, R. F.; Coderre, J. A.; Vicente, M. G. H.; Blue, T. E. Boron neutron capture therapy of cancer: current status and future prospects. *Clin. Cancer Res.* **2005**, *11*, 3987−4002.

(7) Holowka, E. P.; Sun, V. Z.; Kamei, D. T.; Deming, T. J. Polyarginine segments in block copolypeptides drive both vesicular assembly and intracellular delivery. *Nat. Mater.* **2007**, *6*, 52−57.

(8) Cho, K.; Wang, X.; Nie, S.; Chen, Z. G.; Shin, D. M. Therapeutic nanoparticles for drug delivery in cancer. *Clin. Cancer Res.* **2008**, *14*, 1310−1316.

(9) Tong, R.; Cheng, J. Anticancer Polymeric Nanomedicines. *Polym. Rev.* **2007**, *47*, 345−381.

(10) Simon, Y. C.; Ohm, C.; Zimny, M. J.; Coughlin, E. B. Amphiphilic Carborane-Containing Diblock Copolymers. *Macromolecules* **2007**, *40*, 5628−5630.

(11) Gratton, S. E. A.; Parrott, M. C.; Adronov, A. Preparation of Carborane-Containing Polymers by Atom Transfer Radical Polymerization. *J. Inorg. Organomet. Polym. Mater.* **2006**, *15*, 469−475.

(12) Di Meo, C.; Panza, L.; Campo, F.; Capitani, D.; Mannina, L.; Banzato, A.; Rondina, M.; Rosato, A.; Crescenzi, V. Novel types of carborane-carrier hyaluronan derivatives via "click chemistry". *Macromol. Biosci.* **2008**, *8*, 670−681.

(13) Wei, X.; Carroll, P. J.; Sneddon, L. G. Ruthenium-Catalyzed Ring-Opening Polymerization Syntheses of Poly(organodecaboranes): New Single-Source Boron-Carbide Precursors. *Chem. Mater.* **2006**, *18*, 1113−1123.

(14) Benhabbour, S. R.; Parrott, M. C.; Gratton, S. E. A.; Adronov, A. Synthesis and Properties of Carborane-Containing Dendronized Polymers. *Macromolecules* **2007**, *40*, 5678−5688.

(15) Hoyle, C. E.; Bowman, C. N. Thiol-ene click chemistry. *Angew. Chem., Int. Ed.* **2010**, *49*, 1540−1573.

(16) Lowe, A. B. Thiol-ene click reactions and recent applications in polymer and materials synthesis. *Polym. Chem.* **2010**, *1*, 17−17.

(17) Killops, K. L.; Campos, L. M.; Hawker, C. J. Robust, Efficient, and Orthogonal Synthesis of Dendrimers via Thiol-ene "Click" Chemistry. *J. Am. Chem. Soc.* **2008**, *130*, 5062−5064.

(18) Chen, G.; Amajjahe, S.; Stenzel, M. H. Synthesis of thiol-linked neoglycopolymers and thermo-responsive glycomicelles as potential drug carrier. *Chem. Commun.* **2009**, 1198−1200.

(19) Chan, J. W.; Yu, B.; Hoyle, C. E.; Lowe, A. B. Convergent synthesis of 3-arm star polymers from RAFT-prepared poly(N,N-diethylacrylamide) via a thiol-ene click reaction. *Chem. Commun.* **2008**, 4959−4961.

(20) Gu, W.; Chen, G.; Stenzel, M. H. Synthesis of glycomicrospheres via a thiol-ene coupling reaction. *J. Polym. Sci., Part A: Polym. Chem.* **2009**, *47*, 5550−5556.

(21) Jones, M. W.; Mantovani, G.; Ryan, S. M.; Wang, X. X.; Brayden, D. J.; Haddleton, D. M. Phosphine-mediated one-pot thiol-ene "click" approach to polymer-protein conjugates. *Chem. Commun.* **2009**, 5272−5274.

(22) Smith, H. D.; Obenland, C. O.; Papetti, S. A New Series of Organoboranes. IX. The Preparation and Some Reactions of Sulfur-Carborane Derivatives. *Inorg. Chem.* **1966**, *5*, 1013−1015.

(23) Li, G.-Z.; Randev, R. K.; Soeriyadi, A. H.; Rees, G.; Boyer, C.; Tong, Z.; Davis, T. P.; Becer, C. R.; Haddleton, D. M. Investigation into thiol-(meth)acrylate Michael addition reactions using amine and phosphine catalysts. *Polym. Chem.* **2010**, *1*, 1196−1196.

(24) Chu, B. *Laser Light Scattering: Basic Principles and Practice*, 2nd ed.; Academic Press: Boston, MA, 1991.

(25) Pecora, R. *Dynamic Light Scattering: Applications of Photon Correlation Spectroscopy*; Springer 1985.

(26) Laakso, J.; Kulvik, M.; Ruokonen, I.; Vähätalo, J.; Zilliacus, R.; Färkkilä, M.; Kallio, M. Atomic emission method for total boron in blood during neutron-capture therapy. *Clin. Chem.* **2001**, *47*, 1796−1803.
(27) Mehta, S. C.; Lai, J. C.; Lu, D. R. Liposomal formulations containing sodium mercaptoundecahydrododecaborate (BSH) for boron neutron capture therapy. *J. Microencapsulation* **1996**, *13*, 269−279.
(28) Lam, H.; Gong, X.; Wu, C. Novel differential refractometry study of the enzymatic degradation kinetics of poly(ethylene oxide)-b-poly(epsilon-caprolactone) particles dispersed in water. *J. Phys. Chem.* **2007**, *111*, 1531−1535.
(29) Schartl, W. *Light Scattering from Polymer Solutions and Nanoparticle Dispersions*; Springer-Verlag Berlin: Berlin, 2007.
(30) Zhou, S.; Burger, C.; Chu, B.; Sawamura, M.; Nagahama, N.; Toganoh, M.; Hackler, U. E.; Isobe, H.; Nakamura, E. Spherical Bilayer Vesicles of Fullerene-Based Surfactants in Water: A Laser Light Scattering Study. *Science* **2001**, *291*, 1944−1947.
(31) Zhang, G.; Wu, C. The Water/Methanol Complexation Induced Reentrant Coil-to-Globule-to-Coil Transition of Individual Homopolymer Chains in Extremely Dilute Solution. *J. Am. Chem. Soc.* **2001**, *123*, 1376−1380.
(32) Shen, Y.; Jin, E.; Zhang, B.; Murphy, C. J.; Sui, M.; Zhao, J.; Wang, J.; Tang, J.; Fan, M.; Van Kirk, E.; Murdoch, W. J. Prodrugs Forming High Drug Loading Multifunctional Nanocapsules for Intracellular Cancer Drug Delivery. *J. Am. Chem. Soc.* **2010**, *132*, 4259−4265.
(33) Hu, T.; Wu, C. Clustering Induced Collapse of a Polymer Brush. *Phys. Rev. Lett.* **1999**, *83*, 4105−4107.
(34) Hu, T.; Wu, C. Grafting Density Induced Stretching and Collapse of Tethered Poly(ethylene oxide) Chains on a Thermally Sensitive Microgel. *Macromolecules* **2001**, *34*, 6802−6805.
(35) Zhao, H.; Chen, Q.; Hong, L.; Zhao, L.; Wang, J.; Wu, C. What Morphologies Do We Want? − TEM Images from Dilute Diblock Copolymer Solutions. *Macromol. Chem. Phys.* **2011**, *212*, 663−672.
(36) Sumitani, S.; Oishi, M.; Nagasaki, Y. Carborane confined nanoparticles for boron neutron capture therapy: Improved stability, blood circulation time and tumor accumulation. *React. Funct. Polym.* **2011**, *71*, 684−693.